Adsorption of NO, NO2 on Rh Embedded h-BN Monolayer: A First-Principles Study

Jun'an Zhang
Chongqing University of Technology
Jiangling Tian
Chongqing University of Technology
Qingwei Zhang (zhangqingwei@cqut.edu.cn)
Chongqing University of Technology
Yunhua Lu
Chongqing University of Technology
Lei Li
Yangtze Normal University
Yanjie Xu
Chongqing University of Technology

Research Article

Keywords: gas sensing, Rh-doping, h-BN monolayer, adsorption, density functional theory

Posted Date: July 20th, 2021

DOI: https://doi.org/10.21203/rs.3.rs-713339/v1

Adsorption of NO，NO_2 on Rh embedded h-BN monolayer: A first-principles study

Jun'an Zhang[1], Jiangling Tian[1], Qingwei Zhang[1]*, Yunhua Lu[1], Lei Li[2], Yanjie Xu[1]

[1] School of Artificial Intelligence, Chongqing University of Technology, Chongqing, 401135, China

[2] Key Laboratory of Extraordinary Bond Engineering and Advanced Materials Technology (EBEAM) of Chongqing, Yangtze Normal University, Chongqing, 408100, China

*Corresponding author E-mail: zhangqingwei@cqut.edu.cn

Abstract: Density functional theory calculations have been made to investigated the adsorption and sensing properties of harmful nitrogen oxides (NO, NO_2) on rhodium (Rh) doped hexagonal boron nitride (BN) to explore the feasibility of Rh-doped BN (Rh-BN) based gas sensor. For each gas molecule, various adsorption positions and orientations were examined. The favorable adsorption configuration has been established and the corresponding adsorption energy has been calculated. Besides, to understand the adsorption mechanism, The properties such as electron density, the energy band structure, state density of states, and charge transfer of the adsorption system were investigated in greater detail. The calculations indicate that the most stable structure is that the Rh atom located directly above the N atom, and a stable chemical bond with a length of 2.096 Å formed between the Rh atom and N atom, with a significant binding energy (E_b) of -1.561 eV. Then, adsorption performance of Rh-BN monolayer upon nitrogen oxides is in order as NO_2 > NO, with the adsorption energy (E_a) of -3.919 eV and -3.318 eV, respectively. This indicates that the Rh-BN single layer possesses ideal adsorption and sensing properties. Furthermore, by doping the Rh atom, many levels of impurities are introduced into the intrinsic BN band structure, thereby improving the interaction between BN and adsorbed gas molecules. Following adsorption of NO and NO_2, the band gap (E_g) of the doping system is wider. It has been demonstrated that gas adsorption reduces the electrical conductivity of the system, but increases the sensitivity of the system. The above calculation and analysis are of great importance for the exploration of the Rh-BN single layer as innovative gas detection material.

Key words: gas sensing, Rh-doping, h-BN monolayer, adsorption, density functional theory;

1 Introduction

Nitrogen oxides (such as NO and NO_2) as common gaseous pollutant[1, 2], are generally produced from industrial and agricultural production and the combustion of fossil fuels. Not only is NO harmful to the environment, it can also contaminate water bodies, soil and the atmosphere[3]. In addition, NO is readily oxidized into

NO_2 in the air, as a poisonous gas, NO_2 is detrimental to the environment and humans[4]. Excessive inhalation may result in severe damage to cardiorespiratory function[5]. Gas sensors are widely used in many fields, such as civil[6], industrial, and environmental monitoring. For these kinds of harmful gases, it is very important to prepare gas sensors to detect NOx for real-time detection[7–9]. Due to its good stability, high sensitivity to detection, low cost, small volume, and portable belt, the gas-solid sensor offers an extensive field of application[10–12]. However, new materials such as ophtical fibers, semiconductors[3], metal-organic frameworks (MOFs)[13–16], and nanomaterials have been found, which can effectively detect harmful gases, but the detection sensitivity still can't meet the requirements, especially for the detection of corrosive gas molecules like the nitrogen oxides.

Since two-dimensional (2D) nanomaterials such as graphene's isolation[17, 18], they have received considerable research attention due to their excellent strength, flexibility, electrical conductivity, and these outstanding properties make it a research center for gas detection materials. Following the wide application of graphene, 2D materials, including silicene[19, 20], phosphorene[21], and transition metal dichalcogenide[22], also have attracted much attention owing to their fascinating characteristics. Therefore, researchers are devoted to developing new candidate materials with electronic structures and properties similar (or even better) to graphene for many particular applications[23]. BN[24–26], commonly referred as white graphite, is a crystal consisting of atoms N and B, and its structure, together with its properties, are very similar to graphene. Studies have shown that after doping metal atoms in BN, it can act as an emerging and promising sensor nanomaterial. For instance, Xia *et al.* investigated the adsorption of H_2S, SO_2, SOF_2, and SO_2F_2 on Rh-BN monolayer[27]. They found that these gas molecules on Rh-BN belong to chemical adsorption, and Rh-BN endows BN with higher responsiveness and gas detection capacity. Ambrusi *et al.* [28] investigated the stability of graphene boosted by Rh with and without defects. Through the energy analysis of the doping system, Graphene modified by the Rh atom appears to have a good adsorption effect on the H_2 molecule. Other researchers also found that Rh can perform more

effectively than other doped transition metals[29–31]. Therefore, as a suitable metal, Rh adatom can enhance the surface properties of the 2D material monolayer.

In this paper, taking into account the rise of 2D materials similar to graphene in sensing applications, we explored for the first time the Rh-BN as detection material for NO and NO_2. The adsorption process, including adsorption energy, charge density, the density of states (DOS), and band structure, were analyzed by using density functional theory (DFT) based on the first principles. Chapter 2 describes the methodologies and details of the computation process. Chapter 3 provides a detailed analysis and demonstration of NO and NO_2 adsorption on Rh-BN. Chapter 4 deals with the conclusions.

2 Computational methods and models

The electronic properties of NO, NO_2 adsorbed on Rh-BN monolayer are performed within the spin-polarized DFT using the Vienna ab initio simulation package (VASP)[32]. Projector augmented wave (PAW) method is used to describe the electron-ion interactions. To treat electron exchange and correlation, the local density approximation (LDA) overestimates the bond energy of the system and underestimates the bond distance at equilibrium[33, 34], so the generalized gradient approximation (GGA) in the form of Perdew-Burke-Ernzernhof (PBE) is used as the energy exchange-correlation function[35, 36]. A conjugate-gradient algorithm is taken to completely relax the positions of all atoms until the force on the ions is less than 0.02 eV/ Å and the electron self-consistent energy converges to less than 10^{-5} eV. Setting the plane-wave basis with the cutoff energy of 520 eV for structural optimization and subsequent calculations. To avoid the interaction between the periodic images, the vacuum space was kept as 20 Å. In this calculation of the Brillouin zone[37], the Brillouin zone integral was geometrically optimized by using $4 \times 4 \times 1$ k-points Monkhorst-Pack Gamma-centered, and Gaussian smearing broadening is 0.3 eV. The entire system consists of 4×4 BN supercell, including Rh atom doped on BN and individual gas molecules adsorbed on it, the bond length of B-N is 1.451 Å, as shown in Fig.1. This method is used to verify the energy band

structure and density of states of the BN[29], which proves that this method is suitable for the calculation of the BN adsorption system.

For the adsorption systems, the adsorption energy, E_a, between the gas molecules and Rh-BN, is typically defined as:

$$E_a = E_{gas/Rh-BN} - E_{Rh-BN} - E_{gas} \quad (1)$$

where $E_{gas/Rh-BN}$ is the total energy of the gas/Rh-BN, and E_{Rh-BN} and E_{gas} are the total energies of corresponding Rh-BN monolayer and the gas molecule, respectively. The higher the absolute value of E_a, the greater the stability of the corresponding structure. To further explore the electronic properties of adsorption, the charge density difference (CDD) and charge transfer (ΔQ) of the adsorption system were investigated. The charge transfer calculation method of the system is: the amount of charge of each atom in the system is determined by the Bader charge analysis, and the total amount of charge in the system is obtained by accumulation. For the doping system and adsorption system, the charge transfer quantity can be achieved by calculating the amount of charge change before and after doping and adsorption.

3 Results and discussion

3.1 Analysis of Rh-BN monolayer structural properties

To obtain the most stable Rh-BN structure, four highly symmetrical absorbing configurations were considered, including H (the center of BN), B (above the B atom), N (above the N atom), and S (above the B-N bond)[38, 39], as shown in **Fig. 1**. In general, the binding energy (E_b) is used to assess the stability of the structure, which is defined by the following formula (2):

$$E_b = E_{Rh-BN} - E_{Rh} - E_{BN} \quad (2)$$

where E_{Rh-BN} is the energy of Rh-BN, E_{Rh} is the energy of Rh atom, and E_{BN} is the energy of primary BN monolayer. Similar to E_a, the binding energy is negative, and the greater the absolute value of binding energy, the more stable the system is[40].

The optimized structure of Rh-BN is shown in **Fig. 2**, where the Rh atom is

directly above the N atom (at the top of the N atom). The three B-N bonds in the vicinity of the Rh doping are slightly lengthened at 1.47 Å, whereas the measured values of the other B-N bonds in the plane are equal to 1.45 Å in the original system. That is, owing to Rh doping, the N atom of Rh-N bond extends slightly beyond the BN single layer, while the three B atoms that are closest to the Rh dopant do not move during the doping process. Therefore, no significant deformation was observed in the Rh-BN monolayer. The height of Rh atom from the BN plane is 2.096 Å, and the calculated binding energy is -1.561 eV, indicating that this is indicative of relatively stable chemical doping. Moreover, the intrinsic layer of BN is non-magnetic, and the magnetic moments of the system is changed to 1.048 μB due to the presence of unmatched electrons after Rh doping, as shown in **Table. 1**. The CDD of the Rh-BN is shown in **Fig. 3**, The charge density is distributed between the doped Rh atom and the uncoordinated BN monolayer atoms. The electron gain and loss overlap on the Rh-N bond, suggesting the existence of an ideal electron hybridization between the Rh atom and the N atom. Bader charge analysis reveals that there is about 0.14 |e| charge transfer from Rh dopant to BN, suggesting that Rh is electron donor and BN acts as the electron acceptor.

To further explore the behavior of the electrons of the Rh-BN monolayer, the band structures and DOS have also been investigated. For the Rh-BN band structure, some new levels of impurities show up in the band structure near the Fermi level, the band gap (E_g) of BN is 4.656 eV, which is reduced to 1.292 eV after doping the Rh atom, accompanied by binding energy of -1.561 eV, as shown in **Fig. 4**, and the calculated results are consistent with the theoretical values in the literature[27]. Therefore, the electrons of the doped system can easily change from valence band to conduction band, which also explains the lower E_g after doping. Compared with other doped metals[31, 41, 42], The smaller E_b and E_g indicate that the doping effect of the Rh atom at the BN monolayer is improved. For the density of states, **Fig. 5** depicts the total density of states (TDOS) before and after doping. Due to the large E_g of intrinsic BN, the electron distribution near the TDOS Fermi level is zero. The E_g diminishes after doping the Rh atom, and the corresponding peaks appear close to the

Fermi level, indicating that the number of electrons in the doped system increases. Consequently, doping Rh atom can effectively enhance the conductivity of the BN monolayer. Moreover, analysis of the partial wave density of states (PDOS) reveals that the *s* orbital of Rh and the *p* orbital of N have a large overlap at energies from -10 eV to 5 eV, showing a strong orbital hybridization between Rh and N atoms, which also explains the high E_b of the doping system.

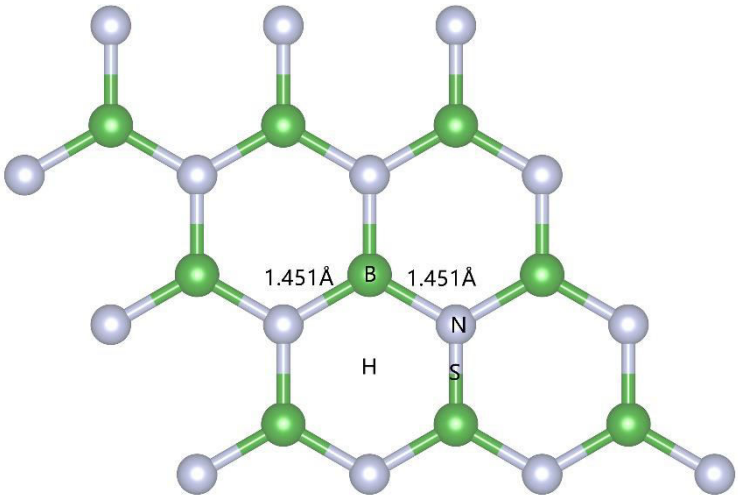

Fig. 1. Structure of original BN. The green spheres represent B atoms, and silver spheres represent N atoms.

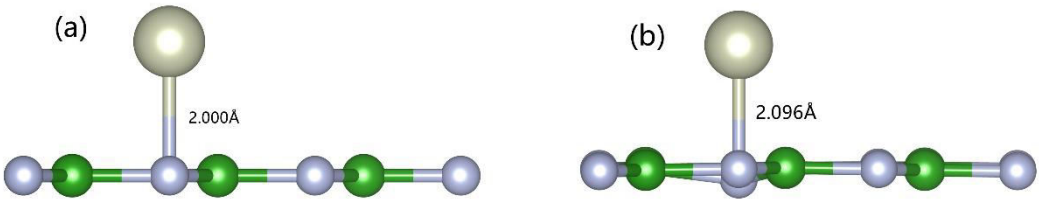

Fig. 2. Doping Rh before optimization from side view(a), Doping Rh after optimization from side view(b). The gray sphere represents Rh atom.

Table 1

Rh doped BN, NO, and NO_2 on Rh-BN: binding energy (E_b), adsorption energy (E_a), adsorption length (d) is defined as the distance between the closest Rh atoms to the substrate surface, the bond length of NO and NO_2 (l_{N-O}) and bond angle ($\Phi_{N\text{-}O}$) after adsorption, charge transfer from the substrate to NO, NO_2 (ΔQ), bandgap (E_g), and magnetic moment of the total system (M).

systems	E_b/E_a (eV)	d(Å)	l_{N-O}(Å)	$\Phi_{N\text{-}O}$(deg)	$\Delta Q(e)$	E_g (eV)	$M_{total}(\mu_B)$
Rh-BN	-1.561	2.096	-	-	0.140	1.292	1.048
Rh-BN/NO_2	-3.919	2.155	1.299	128.668	-0.410	2.043	0.000
Rh-BN/NO	-3.318	2.124	1.176	180	-0.230	1.679	0.000

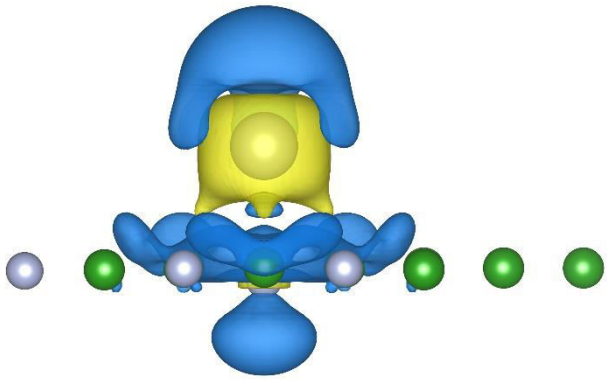

Fig. 3. The CDD for Rh-BN system from the side view. The yellow and blue represent the accumulation and depletion of the electron.

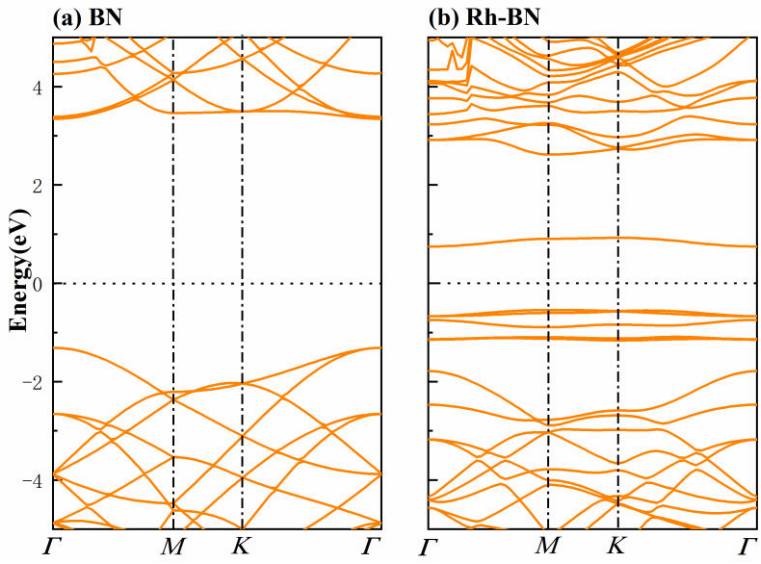

Fig. 4. The band structure of original BN (a) and Rh-BN (b). The dashed line at zero indicates the Fermi level.

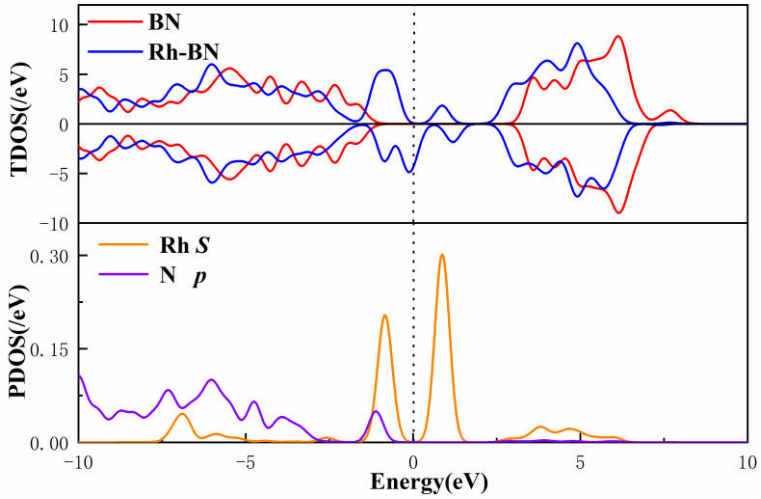

Fig. 5. The total density of states (TDOS) of BN, Rh-BN, and the partial density of states (PDOS) projected on Rh *s* orbitals and N *p* orbitals for the Rh doped BN system. The Fermi level is denoted by dashed line.

3.2 Analysis of Rh-BN/NO_2 adsorption system structural properties

The adsorption behaviour of NO_2 on the optimised Rh-BN monolayer are investigated. NO_2 has four highly symmetrical adsorption positions, and N or O atoms near the substrate should also be taken into consideration. The structure of NO_2 on the Rh-BN (Rh-BN/NO_2) monolayer after geometry optimization is plotted in **Fig. 6**. Originally, the Rh atom is positioned vertically above the N atom. Interestingly, after adsorbing the NO_2 gas molecule, the Rh atom shifts to the inside of hexagonal BN,

the height is increased from 2.000 Å to 2.115 Å, and the adsorption height of Rh-BN/NO_2 is estimated to be 1.850 Å (defined as the shortest molecule-substrate distance), proving that the adsorption gas weakens the binding strength between Rh atom and BN monolayer to a certain extent. The gas adsorption makes the unlinked electrons in the system pair, thus the system magnetism disappears after adsorption. Compared with the original NO_2, after structural optimization, the bond length and bond Angle of NO_2 were increased from 1.204 Å to 1.299 Å and from 120° to 128.668°, respectively. Suggesting that the interaction between N and O atoms in NO_2 is also weakened due to the doping system, which is also in line with the catalytic principle of the catalyst. The calculated adsorption energy is -3.318 eV for NO_2 adsorbed on the Rh-BN monolayer. The large adsorption energy indicates that NO_2 adsorbed Rh-BN is chemisorption. According to Bader charge analysis, NO_2 gas molecule is negatively charged by -0.23 |e| following adsorption. Meaning that the Rh-BN substrate transfers 0.23 charge to the NO_2 gas molecule, from CDD perspective, as shown in **Fig. 7**, electron accumulation occurs around NO_2, which also confirms the behavior of electron acceptance in the surface interaction of gas molecules.

From the energy band structure shown in **Fig. 8**, the changes of energy band structure and E_g before and after adsorption can be observed more directly. Fig. 8(b) plots the energy band of Rh-BN adsorbing NO_2. Compared with the energy band of Rh-BN, new impurity energy levels appear around the Fermi level. During the adsorption process of NO_2, electrons are hardly obtained, showing typical p-type doping characteristics. Findings indicate that the impurity levels are introduced by the NO_2 molecule. It can be seen from the TDOS in **Fig. 9** that the density of states near the Fermi level decreases after gas adsorption. Generally speaking, the conductivity of the adsorption system is dependent on the concentration, species, and mobility of the carriers at the Fermi level. For the system with p-type conductivity, the main carriers are holes. By integrating the density of states curve from Fermi level to Dirac point, the carrier hole concentration can be obtained. As the density of states decreases after adsorption, the corresponding carrier hole concentration will also decrease. According

to the conductivity formula σ=neμ[32], where σ is the conductivity, n is the carrier density of the system, e is the single charge, and μ is the carrier mobility, respectively. As a result, the conductivity of the system is reduced after gas adsorption. Besides, relevant changes in conductivity and sensitivity (s) could be assessed using the following formula $s = \frac{\frac{1}{\sigma_a} - \frac{1}{\sigma_b}}{\frac{1}{\sigma_b}}$, σ_b and σ_a respectively mean the conductivity of single-layer Rh-BN before and after adsorbing gas[43, 44]. Therefore, for the adsorption system, gas adsorption reduces the electrical conductivity of the system but increases its sensitivity. Furthermore, the PDOS of the Rh-BN/NO_2 adsorption system shows that there is a strong hybridization between the *s* orbital of Rh and the *p* orbital of N and O around -10 eV, and the established structure of the adsorption system is stable from another point of view.

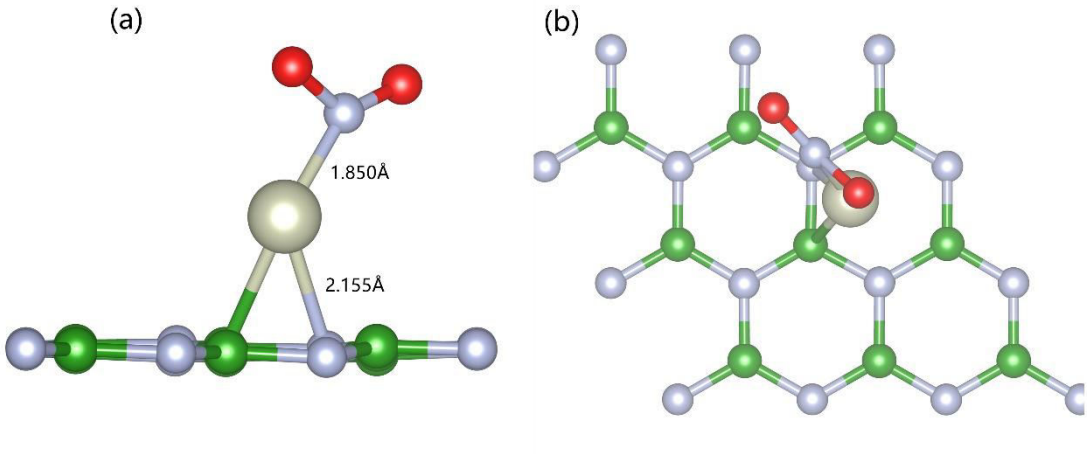

Fig. 6. optimized configurations of Rh-BN/NO_2 from side view (a) and top view (b). The red spheres represent O atoms.

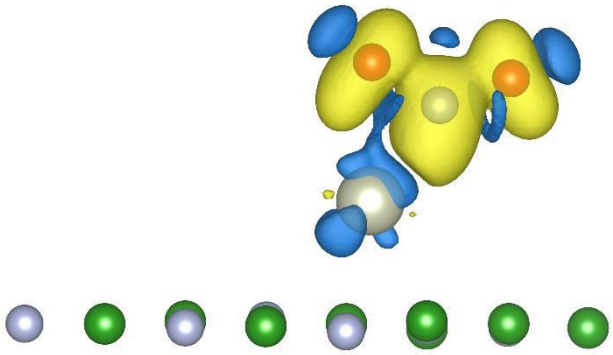

Fig. 7. The CDD of the Rh-BN/NO_2 system from side view.

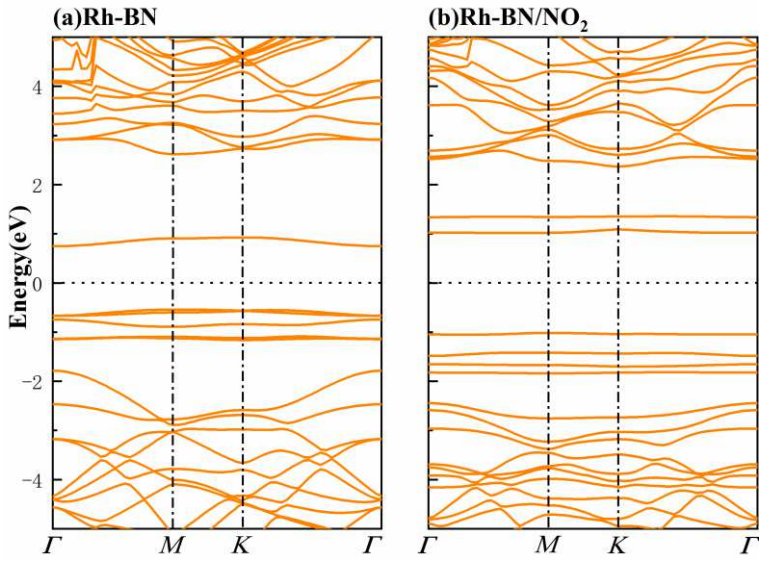

Fig. 8. The band structures of Rh-BN (a) and Rh-BN/NO_2 (b)

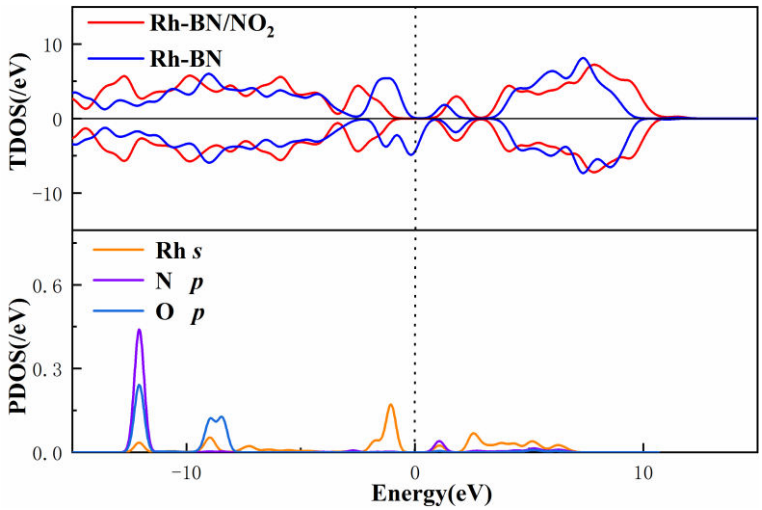

Fig. 9. The TDOS of Rh-BN/NO_2, Rh-BN, and the PDOS projected on Rh *s* orbital, N *p* orbital, and O *p* orbital for Rh-BN/NO_2 system

3.3 Analysis of Rh-BN/NO adsorption system structural properties

Similar to NO_2, for the examination of the most stable adsorption configuration of NO on the Rh-BN monolayer(Rh-BN/NO), NO molecule was initially placed at different positions, including four highly symmetrical adsorption sites, and O and N atoms in the vicinity of the adsorption substrate were also taken into consideration at each site. Following structural optimization, The strongest adsorption configuration of the NO molecule on the Rh-BN layer is shown in the **Fig. 10**. The N atom is found to be close to Rh-BN, the adsorption distance of NO on Rh-BN is 1.712 Å, and the Rh atom slightly moves up to 2.124 Å, However, the structure of the Rh-BN does not change significantly. The calculation of E_a is -3.318 eV, indicating that the NO molecule forms a stable chemical bond with the substrate. Analysis of the load of **Fig. 11** Bader charge shows that approximately 0.41 |e| charge transferred from the doped substrate to the gas molecule NO after adsorption. At this point, NO is acting as an acceptor and Rh-BN is acting as a donor.

To better understand the properties of the Rh-BN/NO system, the DOS and energy band structures are presented on **Fig. 12** and **Fig. 13** respectively. Based on the TDOS analysis, some peaks disappear between -1 eV and 2 eV, this makes it difficult for the electrons to move from the valence band to the conduction band. On the right side of the Femi level, the peak after adsorption of NO is much higher than before

adsorption. This causes E_g to increase to various degrees, whose Rh-BN/NO Eg increases to 1.679 eV after NO gas adsorption. The conclusions drawn by TDOS and energy band structures are consistent. Besides, for the band structure, impurity energy levels appear at the energy levels of -3 eV and -2 eV after adsorption NO, indicating that the conductivity of the adsorption system changes significantly after absorption. From the above analyses, the E_g is inversely proportional to the conductivity and directly proportional to the sensitivity. Thus, although NO adsorption reduces Rh-BN conductivity, the sensitivity of the adsorption system is improved to some extent. The PDOS suggests that the *s* orbital of Rh has a strong hybridization with *p* of N and O, demonstrating the there is a stable binding force between Rh-BN and NO. Consequently, the high E_a and the stable geometric structure of the RH-BN/NO adsorption system are explained as well.

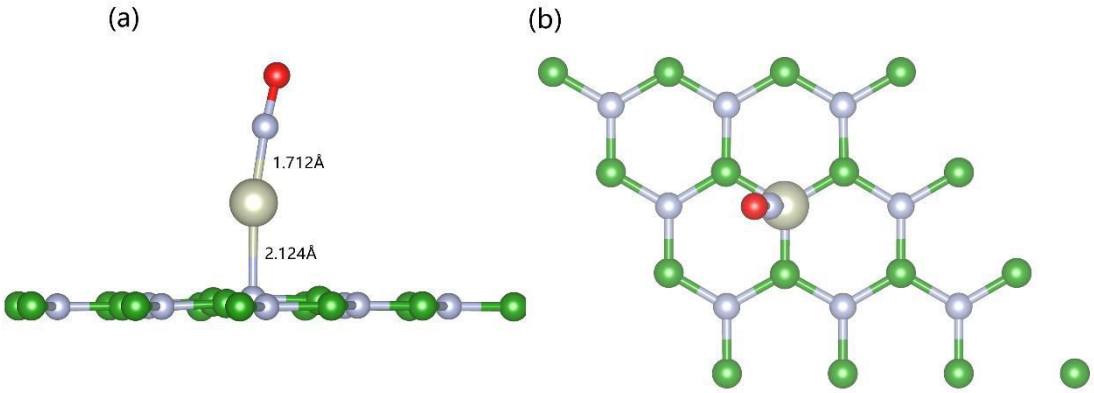

Fig. 10. Optimized configurations of Rh-BN/NO from side view (a) and top view (b).

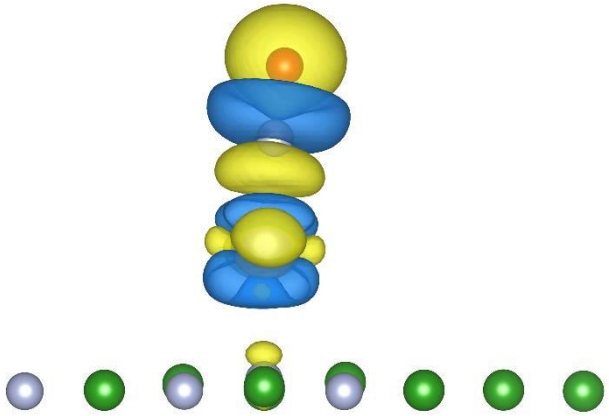

Fig. 11. The CDD of Rh-BN/NO system from the side view.

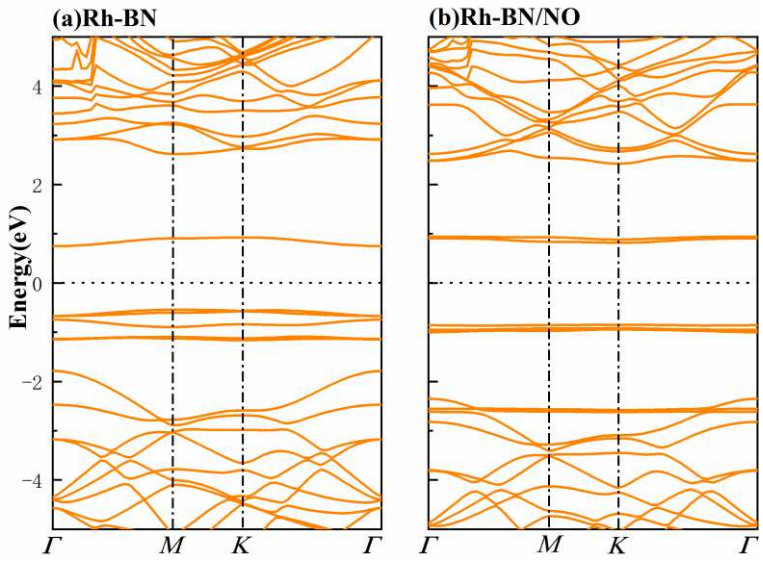

Fig. 12. The band structures of Rh-BN (a) and Rh-BN/NO (b)

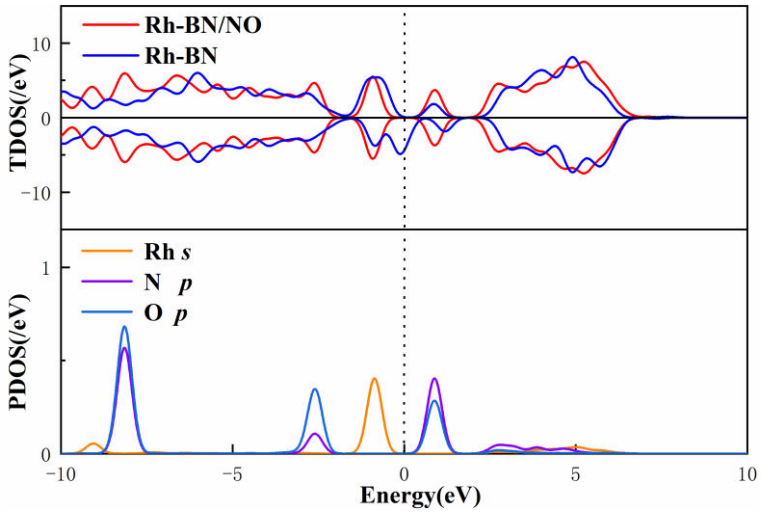

Fig. 13. The TDOS of Rh-BN/NO, Rh-BN, and the PDOS projected on Rh *s* orbitals, N *p* orbitals, and O *p* orbitals for Rh-BN/NO system

4 Conclusions

Two-dimensional monolayer compounds have potential applications in gas sensing due to their unique properties. In this paper, via *ab initio* simulations we have thoroughly investigated the adsorption, magnetic, and electronic behaviors of small gas molecules (NO, NO_2) on BN monolayer embedded with transition metal elements. It can be observed that after the structure optimization, the adsorption locations and heights of NO and NO_2 are changed. The bond lengths of NO and NO_2 increase from 1.166 Å and 1.204 Å to 1.176 Å and 1.299 Å, respectively, indicating that the substrate will weaken the interaction between gas molecules. Interestingly, the original BN monolayer exhibits non-magnetic behavior, but the system has a magnetic moment of 1.048 μ_B after doping the metal Rh. The E_a of NO and NO_2 are -3.318 eV and -3.919 eV, respectively. The higher E_a indicates that stable chemical bonds are formed between the gas molecule and the Rh-BN monolayer, therefore, the adsorption process belongs to the strong chemical adsorption. By analyzing the Bader charge, it is found that for the Rh-BN system, the charge transfer between Rh dopant and BN monolayer is 0.14 |e|, while the charge transfer between Rh-BN monolayer and adsorbed NO and NO_2 is -0.23 |e| and -0.41|e| respectively. In other words, Rh dopant acts as a donor to transfer 0.14 |e| charges to the substrate, whereas in the adsorption system, NO and NO_2 act as a donor to transfer 0.23 |e| and 0.41 |e| electrons to the

substrate, respectively. In NO and NO_2 systems, Rh dopants hybridized with typical atoms in the adsorbed gas to form some new energy bands. By analyzing the TDOS diagram of the adsorption system, it can be seen that the carrier concentration of the system decreases after the adsorption of gas, leading to the decrease of the electrical conductivity of the system, and increase of the sensitivity of the system to detect gas. Our calculations found that, in general, the embedded transition metal significantly enhances the chemical reactivity of the BN monolayer, allowing the substrate to better react with adsorbed gas molecules, suggesting that BN has great potential in gas sensing.

Funding

This research was funded by the Science and Technology Research Program of Chongqing Municipal Education Commission (KJQN201901108), the Scientific Research Foundation of Chongqing University of Technology (2019ZD06, 2020ZDZ026), and the Postgraduate Innovation Program of Chongqing University of Technology (clgycx20202120).

Conflicts of interest

There are no conflicts to declare.

Availability of data and material

The data used to support the findings of this study are available from the corresponding author upon request.

Code availability

Vienna ab-initio simulation package program.

Authors' contributions

Jiangling Tian: Conceptualization, Methodology, Writing-Original draft preparation, Writing-Reviewing and Editing; Yanjie Xu, Lei Li: Investigation; Jun'an Zhang, Qingwei Zhang and Yunhua Lu: Supervision.

Reference

1. Li H-Y, Cai Z-X, Ding J-C, Guo X (2015) Gigantically enhanced NO sensing

properties of WO3/SnO2 double layer sensors with Pd decoration. Sensors and Actuators B: Chemical 220:398–405. https://doi.org/10.1016/j.snb.2015.05.091

2. Delaria ER, Vieira M, Cremieux J, Cohen RC (2018) Measurements of NO and NO2 exchange between the atmosphere and Quercus agrifolia. Atmos Chem Phys 18:14161–14173. https://doi.org/10.5194/acp-18-14161-2018

3. Fine GF, Cavanagh LM, Afonja A, Binions R (2010) Metal Oxide Semi-Conductor Gas Sensors in Environmental Monitoring. Sensors 10:5469–5502. https://doi.org/10.3390/s100605469

4. Leenaerts O, Partoens B, Peeters FM (2008) Adsorption of H2O , NH3 , CO, NO2 , and NO on graphene: A first-principles study. Phys Rev B 77:125416. https://doi.org/10.1103/PhysRevB.77.125416

5. Pacher P, Beckman JS, Liaudet L (2007) Nitric Oxide and Peroxynitrite in Health and Disease. Physiological Reviews 87:315–424. https://doi.org/10.1152/physrev.00029.2006

6. Tian W, Liu X, Yu W (2018) Research Progress of Gas Sensor Based on Graphene and Its Derivatives: A Review. Applied Sciences 8:1118. https://doi.org/10.3390/app8071118

7. Liu X, Cheng S, Liu H, et al (2012) A Survey on Gas Sensing Technology. Sensors 12:9635–9665. https://doi.org/10.3390/s120709635

8. Basu S, Bhattacharyya P (2012) Recent developments on graphene and graphene oxide based solid state gas sensors. Sensors and Actuators B: Chemical 173:1–21. https://doi.org/10.1016/j.snb.2012.07.092

9. Ratchagar NP, Fidal VT, Bhadra P, et al (2019) Sensor for Continuous and Real-Time Monitoring of Biomolecule Permeation Through Ultrathin Silicon Nanoporous Membranes. IEEE Sensors J 19:4419–4427. https://doi.org/10.1109/JSEN.2019.2900285

10. Govardhan K, Grace AN (2016) Metal/Metal Oxide Doped Semiconductor Based Metal Oxide Gas Sensors—A Review. sens lett 14:741–750. https://doi.org/10.1166/sl.2016.3710

11. Li J, Xu S, Tang Z, et al (2020) Electrostatic Coupled Capacitance Sensor for Gas Solid Flow Measurement. IEEE Sensors J 20:12807–12816. https://doi.org/10.1109/JSEN.2020.3001689

12. dos Reis E, de Andrade MFF, Albuquerque GM, et al (2021) Characterization of gas-solid flow in a cold fluidized bed from signals of a non-invasive electrical charge sensor. Powder Technology 382:512–523. https://doi.org/10.1016/j.powtec.2021.01.016

13. Gadipelli S, Ford J, Zhou W, et al (2011) Nanoconfinement and Catalytic Dehydrogenation of Ammonia Borane by Magnesium-Metal–Organic-Framework-74. Chem Eur J 17:6043–6047. https://doi.org/10.1002/chem.201100090

14. Peng WY, Wang Y, Cassady SJ, et al (2019) Single-Ended Sensor for Thermometry and Speciation in Shock Tubes Using Native Surfaces. IEEE Sensors J 19:4954–4961. https://doi.org/10.1109/JSEN.2019.2903989

15. Lei C, Gao J, Ren W, et al (2019) Fabrication of metal-organic frameworks@cellulose aerogels composite materials for removal of heavy metal ions in water. Carbohydrate Polymers 205:35–41. https://doi.org/10.1016/j.carbpol.2018.10.029

16. Zhang M, Lu W, Li J-R, et al (2014) Design and synthesis of nucleobase-incorporated metal–organic materials. Inorg Chem Front 1:159. https://doi.org/10.1039/c3qi00042g

17. Mei L, Zhu S, Yin W, et al (2020) Two-dimensional nanomaterials beyond graphene for antibacterial applications: current progress and future perspectives. Theranostics 10:757–781. https://doi.org/10.7150/thno.39701

18. Varghese S, Varghese S, Swaminathan S, et al (2015) Two-Dimensional Materials for Sensing: Graphene and Beyond. Electronics 4:651–687. https://doi.org/10.3390/electronics4030651

19. Zhao J, Liu H, Yu Z, et al (2016) Rise of silicene: A competitive 2D material. Progress in Materials Science 83:24–151. https://doi.org/10.1016/j.pmatsci.2016.04.001

20. Pi X, Ni Z, Liu Y, et al (2015) Density functional theory study on boron- and phosphorus-doped hydrogen-passivated silicene. Phys Chem Chem Phys 17:4146–4151. https://doi.org/10.1039/C4CP05196C

21. Zhang W, Huynh T, Xiu P, et al (2015) Revealing the importance of surface morphology of nanomaterials to biological responses: Adsorption of the villin headpiece onto graphene and phosphorene. Carbon 94:895–902. https://doi.org/10.1016/j.carbon.2015.07.075

22. Wu S, Du Y, Sun S (2017) Transition metal dichalcogenide based nanomaterials for rechargeable batteries. Chemical Engineering Journal 307:189–207. https://doi.org/10.1016/j.cej.2016.08.044

23. Yang Y, Hou H, Zou G, et al (2019) Electrochemical exfoliation of graphene-like two-dimensional nanomaterials. Nanoscale 11:16–33. https://doi.org/10.1039/C8NR08227H

24. Neek-Amal M, Beheshtian J, Sadeghi A, et al (2013) Boron Nitride Monolayer: A Strain-Tunable Nanosensor. J Phys Chem C 117:13261–13267. https://doi.org/10.1021/jp402122c

25. Li Y, Zhang W, Guo B, Datta D (2017) Interlayer shear of nanomaterials: Graphene–graphene, boron nitride–boron nitride and graphene–boron nitride. Acta Mechanica Solida Sinica 30:234–240. https://doi.org/10.1016/j.camss.2017.05.002

26. Weng Q, Wang X, Wang X, et al (2016) Functionalized hexagonal boron nitride nanomaterials: emerging properties and applications. Chem Soc Rev 45:3989–4012. https://doi.org/10.1039/C5CS00869G

27. Xia S-Y, Tao L-Q, Jiang T, et al (2021) Rh-doped h-BN monolayer as a high sensitivity SF6 decomposed gases sensor: A DFT study. Applied Surface Science 536:147965. https://doi.org/10.1016/j.apsusc.2020.147965

28. Ambrusi RE, Luna CR, Juan A, Pronsato ME (2016) DFT study of Rh-decorated pristine, B-doped and vacancy defected graphene for hydrogen adsorption. RSC Adv 6:83926–83941. https://doi.org/10.1039/C6RA16604K

29. Ma S, Li D, Rao X, et al (2020) Pd-doped h-BN monolayer: a promising gas scavenger for SF6 insulation devices. Adsorption 26:619–626. https://doi.org/10.1007/s10450-020-00226-3

30. Chen X, Zang W, Vimalanathan K, et al (2013) A versatile approach for decorating 2D nanomaterials with Pd or Pt nanoparticles. Chem Commun 49:1160–1162. https://doi.org/10.1039/C2CC37606G

31. Li D, Li W, Zhang J (2020) Fe doped BN monolayer: A promising low-cost single atom catalyst for promoted CO oxidation activity. Applied Surface Science 525:146567. https://doi.org/10.1016/j.apsusc.2020.146567

32. Das NK, Shoji T (2011) A density functional study of atomic oxygen and water molecule adsorption on Ni(111) and chromium-substituted Ni(111) surfaces. Applied Surface Science 258:442–447. https://doi.org/10.1016/j.apsusc.2011.08.107

33. Stampfl C, Mannstadt W, Asahi R, Freeman AJ (2001) Electronic structure and physical properties of early transition metal mononitrides: Density-functional theory LDA, GGA, and screened-exchange LDA FLAPW calculations. Phys Rev B 63:155106. https://doi.org/10.1103/PhysRevB.63.155106

34. Jaffe JE, Snyder JA, Lin Z, Hess AC (2000) LDA and GGA calculations for high-pressure phase transitions in ZnO and MgO. Phys Rev B 62:1660–1665. https://doi.org/10.1103/PhysRevB.62.1660

35. Perdew JP, Burke K, Ernzerhof M (1996) Generalized Gradient Approximation Made Simple. Phys Rev Lett 77:3865–3868. https://doi.org/10.1103/PhysRevLett.77.3865

36. Xiao H, Shin H, Goddard WA (2018) Synergy between Fe and Ni in the optimal performance of (Ni,Fe)OOH catalysts for the oxygen evolution reaction. Proc Natl Acad Sci USA 115:5872–5877. https://doi.org/10.1073/pnas.1722034115

37. Monkhorst HJ, Pack JD (1976) Special points for Brillouin-zone integrations. Phys Rev B 13:5188–5192. https://doi.org/10.1103/PhysRevB.13.5188

38. Cui Z, Wang X, Ding Y, et al (2020) Adsorption of CO, NH3, NO, and NO2 on pristine and defective g-GaN: Improved gas sensing and functionalization. Applied Surface Science 530:147275. https://doi.org/10.1016/j.apsusc.2020.147275

39. Herrera-Rodríguez F, Martínez-Aguilar E, Guerrero-Sánchez J, et al (2019) Oxygen adsorption on Graphene/GaN (0001) surface: A first-principles study. Surface Science 690:121481. https://doi.org/10.1016/j.susc.2019.121481

40. Peyghan AA, Noei M, Yourdkhani S (2013) Al-doped graphene-like BN nanosheet as a sensor for para-nitrophenol: DFT study. Superlattices and Microstructures 59:115–122. https://doi.org/10.1016/j.spmi.2013.04.005

41. Wang G, Yu J, Zheng K, et al (2020) A Monolayer Composite of h-BN Doped by a Nano Graphene Domain: As Sensitive Material for SO2 Gas Detection. IEEE Electron Device Lett 41:1404–1407. https://doi.org/10.1109/LED.2020.3008556

42. Gui Y, Li T, He X, et al (2019) Pt Cluster Modified h-BN for Gas Sensing and Adsorption of Dissolved Gases in Transformer Oil: A Density Functional Theory Study. Nanomaterials 9:1746. https://doi.org/10.3390/nano9121746

43. Vilé G, Albani D, Nachtegaal M, et al (2015) A Stable Single-Site Palladium Catalyst for Hydrogenations. Angew Chem Int Ed 54:11265–11269. https://doi.org/10.1002/anie.201505073

44. Wang X, Zhi C, Li L, et al (2011) “Chemical Blowing” of Thin-Walled Bubbles: High-Throughput Fabrication of Large-Area, Few-Layered BN and Cx-BN Nanosheets. Adv Mater 23:4072–4076. https://doi.org/10.1002/adma.201101788